Metagenomic and Metabonomic Profiling provide insights into AIDS resistance in African Green Monkey

Xiao-jun Zhou
Laboratory Animal Center, Academy of Military Medical Sciences
Jin Wang
Laboratory Animal Center, Academy of Military Medical Sciences
Yan-jiao Shang
Laboratory Animal Center, Academy of Military Medical Sciences
Shuang Wang
Laboratory Animal Center, Academy of Military Medical Sciences
Yefeng Qiu (qiuyefeng2001@163.com)
Laboratory animal center, academy of military medical sciences https://orcid.org/0000-0002-5392-3293
Zheng Yuan (yuanzheng001@126.com)
Laboratory Animal Center, Academy of Military Medical Sciences

Research

Keywords: African green monkey, SIV resistance, microbiome, metabolite

Posted Date: August 24th, 2020

DOI: https://doi.org/10.21203/rs.3.rs-60980/v1

Abstract

Background

As a natural host of simian immunodeficiency virus (SIV), African green monkeys (AGM) do not develop AIDS. AGM has recently been shown to rapidly activate and maintain evolutionarily conserved regenerative wound healing mechanisms in mucosal tissue in case of SIV acute infection, suggesting a role of mucosal integrity in AIDS resistance.However, little is known about the underlying mechanisms, especially of which the gut microbiome as well as the metabolites participate in. This study aims to characterize the profiles of gut microbiome and metabolites of AGM with chronic SIV infection (AGM_P), AGM without SIV infection (AGM_N), Cynomolgus macaque (CM), Rhesus macaque (RM).

Results

Compared with CM and RM, significant decreases in the abundances of *Streptococcus*, *Alistipes*, *Treponema*, *Bacteoides*, *Methanobrevibacter*, *Methanobrevibacter* ($P < 0.01$), as well as significant increases in the abundances of *Clostridium*, *Eubacterium*, *Blautia*, *Roseburia*, *Faecalibacterium*, *Dialister* ($P < 0.01$) were demonstrated in AGM_N. Compared with AGM_N, a trend in the increased abundances of *Streptococcus* and *Roseburia* were found in AGM_P. Quantitative RT-PCR analysis validated the increased abundances of butyrate-producing *Faecalibacterium prausnitzii* and *Eubacteria* in AGM_N ($P < 0.05$). Metabolites involved in lipid metabolism, as well as in butanoate metabolism, were found to be with significantly different levels between AGM_P, AGM_N and CM. And some of these metabolites were shown to be correlated to the abundances of Haloarchaeobius, Methanobrevibacter, Methanothermococcus, and Methanoregula in AGM_N and AGM_P.

Conclusions

Compared with CM and RM, AGM possesses different capacities of lipid metabolism and butanoate metabolism, which correlates with gut homeostasis and mucosal integrity. These findings may provide insight into AIDS resistance in AGM.

Background

The gut is home of trillions of bacteria which outnumber the number of host cells by a factor of 10 to 1 [1]. Accumulating evidence has pointed out a potent role of this microbial community in shaping physiology on host metabolism [2], autoimmune and allergic inflammation [3, 4], enteric immunity [5], and communication with the CNS [6, 7]. Furthermore, a link between variations in microbiome composition and reduced efficacy in various immune interventions, including prevention of HIV infection [8] and anti-PD1 cancer immunotherapy [9, 10].

Although rodent models are most frequently used to establish causality between a given variation of the gut microbiota and disease, several studies have demonstrated that the mouse gut microbiome differs greatly from that of humans [11–13]. Non-human primates (NHPs) have been vital for medical research due to their close evolutionary relationship, similar behavioral and physiological characteristics to humans. Three of the most commonly used NHPs are Rhesus macaque (*Macaca muluta*), Cynomolgus macaque (*Macaca fascicularis*) and African green monkey (*Chlorocebus Sabaeus*), which are widely used in studies of neuroscience, infectious diseases and drug safety testing [14–18]. Differences also exist between these species. For example, AGM has been known to exhibit AIDS resistance in case of simian immunodeficiency virus (SIV) infection [19, 20]. Also, AGM develops spontaneous hypertension with pathophysiological changes that mimic those of patients with essential hypertension [21, 22]. Research has also shown that genetic factors influence the atherogenic response of lipoproteins to dietary fat and cholesterol in nonhuman primates which reflects different capacities in lipid metabolism between AGM and CM [23]. A recent study found that AGM rapidly activate and maintain evolutionarily conserved regenerative wound healing mechanisms in mucosal tissue, which preserves mucosal integrity and prevents inflammatory insults that underlie immune exhaustion in RMs [24]. Role of the gut microbiome and metabolites in shaping these differences as well as the underlying mechanisms needs to be investigated.

Previous studies have almost explored the gut microbiota of different monkey species using 16S rRNA gene amplicon sequencing, of which little information on gene identity and function of the gut microbiome was revealed [25–28]. This study aims to compare profiles the gut microbiome and metabolites of AGM_P, AGM_N, CM and RM through metagenomic and metabonomic sequencing.

Methods

Animals, sample collection, and transportation

A colony of captive AGM were obtained from the Republic of Uganda and raised in our center. Animals were housed in troop enclosures with an outdoor facility and fed nonhuman primate chow per day and a combination of fresh bananas, apples, carrots 3 days per week. All protocols were in strict accordance with the recommendations in the Guide for the Care and Use of Laboratory Animals. Fresh feces from 8 SIV- AGM, 8 SIV + AGM, 10 SIV- CM, and 10 SIV-RM with the age between 5–10 years old were chosen for metagenomic and metabonomic sequencing. Fresh feces were collected, immediately frozen, kept on dry ice during transportation to NovoGene (Tianjin, China) for further processing.

DNA extraction, library construction and sequencing

DNA extraction of a frozen aliquot (200 mg) of each fecal sample was performed by MagPure Stool DNA KF kit B (Magen, China) following manufacturer's introduction. The concentration of fecal DNA was measured by a Qubit Fluorometer by using Qubit dsDNA BR Assay kit (Invitrogen, USA) and further estimated by agarose gel electrophoresis. A total amount of 1 μg DNA per sample was used as input

material for the DNA sample preparations. Sequencing libraries were generated using NEBNext® Ultra™ DNA Library Prep Kit for Illumina (NEB, USA) following manufacturer's recommendations. The DNA sample was fragmented by sonication to a size of 350 bp, end-polished, A-tailed, and ligated with the full length adaptor for Illumina sequencing with further PCR amplification. The PCR products were purified (AMPure XP system) and libraries were analysed for size distribution by Agilent 2100 Bioanalyzer. The clustering of the index-coded samples was performed on a cBot Cluster Generation System according to the manufacturer's instructions. After cluster generation, the library preparations were sequenced on an Illunima HiSeq platform and paired-end reads were generated.

Metagenomic Assembly, gene prediction and abundance analysis

Raw reads were filtered with a quality-control cutoff (adapter sequence < 15 bp, "N" base < 10 bp, Q > 20, final length > 40). The host genome Chlorocebus_sabeus 1.1 (NCBI accession no.GCA_000409795.2), rheMacS_CGG.01 (NCBI accession no.GCA_008058575.1) and Macaca_fascicularis_5.0 ((NCBI accession no.GCA_000364345.1) were chosen for construction of the gene catalog, respectively. Clean data was assembled and analyzed by SOAPdenovo software (V2.04, http://soap.genomics.org.cn/soapfenovo.html). ORF of the Scaftigs (≥ 500 bp) assembled were predicted by MetaGeneMark (V2.10, http://topaz.gatech.edu/GeneMark/) software. For predicted ORF, CD-HIT (CD-HIT, RRID:SCR_007105) [29] was used for construction of an NR geneset by pairwise comparison of all genes in all samples.

Taxonomy prediction

DIAMOND software [30] (V0.9.9, http://github.com/bbuchfink/diamond/), was used to blast the Unigenes to the sequences of Bacteria, Fungi, Archaea and Viruses which were all extracted from the NR database (Version:2018-01-02, http://www.ncbi.nlm.nih.gov) of NCBI. Krona analysis, the exhibition of generation situation of relative abundance, the exhibition of abundance cluster heat map, PCA (R ade4 package, Version 2.15.3) and NMDS (R vegan package, Version 2.15.3) decrease-dimension analysis were based on the abundance table of each taxonomic hierarchy. Differences between groups were tested by Anosim analysis (R vegan package, Version 2.15.3). Metastats and LEfSe analysis were used to look for the different species between groups. Permutation tests between groups were used in Metastats analysis for each taxonomy and Benjamini and Hochberg False Discovery Rate was used for correction of the P value and acquire q value. LEfSe analysis was conducted by LEfSe software. Finally, random forest (R pROC and randomForest packages, Version 2.15.3) was used to construct a random forest model.

Common functional database annotations

The nucleotide sequences of the gene catalog were translated into amino acid sequences and aligned against the proteins or domains in eggNOG database (2015-10), CAZy database (2017-09), COG database (2014-11), Swiss-prot database (2017-07), the KEGG database (89.1) and CARD database (4.0) by DIAMOND with an E value cutoff of 1e − 5. KEGG annotation was performed using an in-house pipeline, where each protein was assigned to a KO when the highest-scoring annotated hit contained at

least one alignment over 60 hits.Resistance gene annotation was performed by aligning the Unigenes to CARD database (http://card.mcmaster.ca/).

KEGG pathway enrichment analysis and rarefaction curve analysis

One-tailed Wilcoxon rank-sum test was performed for all the KOs that occured in more than five samples and adjusted for multiple testing using the Benjamin-Hochberg procedure. Calculations of the Z-score, the aggregated Z-score for a KEGG pathway, the adjusted Z-score for a KEGG pathway were performed as described [31]. A reporter score of ≥ 1.6 (90% confidence according to normal distribution) could be used as a detection threshold for significantly differentiating pathways. Rarefaction analysis was performed to assess the gene richness.

Within sample diversity

Based on the species profile, within sample (alpha & beta) diversity was calculated to estimate the species richness of a sample. Shannon index was used for quantizing the alpha diversity with the formula as described [32]. The beta diversity was calculated using Bray-Curtis distance [33].

Analysis of the microbiome through Real-Time Quantitative Reverse-Transcription Polymerase Chain Reaction

Fresh feces from 20 SIV- AGM and 20 SIV- CM as well as those of 8 SIV- AGM and 8 SIV + AGM were extracted by QIAamp Fast DNA Stool Mini Kit (Qiagen). Relative abundance of the selected bacterial population were analysed through SYBR-based quantitative PCR with an CFX real-time PCR systems (Bio-rad). The primer sets specific for each bacteria are shown in Table 1.

Table 1
Sequences of the primers used in the SYBR-green-based quantitative RT-PCR validation.

Primer name	Primer sequence (5'–>3')
Prevotella-F	5'GAAGGTCCCCACATTG3'
Prevotella-R	5' CAATCGGAGTTCTTCGTG3'
F.prausnitzii-F	5'GATGGCCTCGCGTCCGATTAG3'
F.prausnitzii-R	5'CCGAAGACCTTCTTCCTCC3'
Bifidobacterium-F	5'GGGTGGTAATGCCGGATG3'
Bifidobacterium-R	5'TAAGCCATGGACTTTCACACC3'
Enterobacteriaceae-F	5'CATTGACGTTACCCGCAGAAGAAGC3'
Enterobacteriaceae-R	5'CTCTACGAGACTCAAGCTTGC3'
Eubacterium-F	5'ACTCCTACGGGAGGCAGCAGT3'
Eubacterium-R	5'ATTACCGCGGCTGCTGGC3'
Lactobacillus-F	5' AGCAGTAGGGAATCTTCCA3'
Lactobacillus-R	5' ATTTCACCGCTACACATG3'

Metabolites Extraction

Feces (100 mg) were individuallly grounded with liquid nitrogen and the homogenate was resuspended with prechilled 80% methanol and 0.1% formic acid by well vortexing. The samples were incubated on ice for 5 min and then centrifuged at 15000 rpm, 4℃ for 5 min. Some of the supernatant was diluted to final concentration containing 53% methanol by LC-MS grade water. The samples were subsequently transfered to a fresh Eppendorf tube and then centrifuged at 15000 g, 4 ℃ for 10 min. Finally, the supernatant was injected into the LC-MS/MS system analysis.

UHPLC-MS/MS Analysis

UHPLC-MS/MS analyses were performed using a Vanquish UHPLC system (Thermo Fisher, Germany) coupled with an Orbitrap Q Exactive™ HF mass spectrometer (Thermo Fisher, Germany) in Novogene Co., Ltd. (Beijing, China). Samples were injected onto a Hypesil Gold column (100 × 2.1 mm, 1.9 μm) using a 17-min linear gradient at a flow rate of 0.2 mL/min. The eluents for the positive polarity mode were eluent A (0.1% FA in water) and eluent B (Methanol). The eluents for the negative polarity mode were eluent A (5 mM ammonium acetate, pH 9.0) and eluent B (Methanol). The solvent gradient was set as follows:2% B, 1.5 min; 2-100% B, 12.0 min; 100% B, 14.0 min; 100-2% B, 14.1 min; 2% B, 17 min. Q Exactive™ HF mass

spectrometer was operated in positive/negative polarity mode with spray voltage of 3.2 kV, capillary temperature of 320 ℃, sheath gas flow rate of 40 arb and aux gas flow rate of 10 arb.

Data processing and metabolite identification

The raw data files generated by UHPLC-MS/MS were processed using the Compound Discoverer 3.1 (CD3.1, Thermo Fisher) to perform peak alignment, peak picking, and quantitation for each metabolite. The main parameters were set as follows: retention time tolerance, 0.2 min; actual mass tolerance, 5 ppm; signal intensity tolerance, 30%; signal/noise ratio, 3; minimum intensity, 100,000. After that, peak intensities were normalized to the total spectral intensity. The normalized data was used to predict the molecular formula based on additive ions, molecular ion peaks and fragment ions. And then peaks were matched with the mzCloud (http://www.mzcloud.org), mzVault and MassList database to obtain the accurate qualitative and relative quantitative results. Statistical analyses were performed using the statistical software R (R version R-3.4.3), Python (Python 2.7.6 version) and CentOS (CentOS release 6.6). When data were not normally distributed, normal transformations were attempted using area normalization method.

Data Analysis of the Untargeted Metabolomics

These metabolites were annotated using the KEGG database (http://www.genome,jp/kegg/pathway.html), HMDB database (http://hmdb.ca/metabolites). Principal components analysis (PCA) and Partial least squares discriminant analysis (PLS-DA) were performed at metaX (a flexible and comprehensive software for processing metabolomics data). We applied univariate analysis (t-test) to calculate the statistical significance (P-value). The metabolites with VIP > 1 and P-value < 0.05 and fold change (FC) ≥ 2 or FC ≦ 0.5 were considered to be differential metabolites.

For clustering heat map, the data were normalized using z-scores of the intensity areas of differential metabolites and were ploted by Pheatmap package in R language. The correlation between differential metabolites were analyzed by cor () in R language with the pearson method. Statistically significant of correlation between differential metabolites were calculated by cor.mtest () in R language. P-value < 0.05 was considered as statistically significant and correlation plots were ploted by corrplot package in R language. The functions of these metabolites and metabolic pathways were studied using the KEGG database. The metabolic pathways enrichment of differential metabolites was performed. When ratio were satisfied by x/n > y/n, metabolic pathway were considered as enrichment. When P-value of metabolic pathway < 0.05, metabolic pathway were considered as statistically significant enrichment.

Statistical Analysis

Values were expressed as mean ± SD. The comparative CT method was used in real-time qRT-PCR assay according to the delta-delta CT method. Statistical analyses were performed using GraphPad Prism version 5.01. t test and Wilcoxon rank sum test were used to compared statistical differences. The data were considered statistically significant at $P < 0.05$.

Results

Comparison of the gut microbiota profiles between AGM_N, CM, RM

Rarefaction analysis based on the core and pan gene numbers of the samples was performed which both demonstrated a curve approaching saturation (Fig.S1). Based on taxonomical annotation, composition of the microbiota at the phylum level varied with a higher abundance of *Bacteroidetes* in CM, a higher abundance of *Spirochaetes* in RM, and a higher abundance of *Actinobacteria* in AGM_N (Fig.S2). Composition of the microbiota at the genus level also varied between different groups (Fig. 1&S3). Compared with CM and RM, significant decrease in the abundances of *Streptococcus*, *Alistipes*, *Treponema*, *Bacteoides*, *Methanobrevibacter*, *Methanobrevibacter* ($P < 0.01$), as well as significant increase in the abundances of *Clostridium*, *Eubacterium*, *Blautia*, *Roseburia*, *Faecalibacterium*, *Dialister* ($P < 0.01$) were demonstrated in AGM_N (Fig. 1&S3). Cluster analysis of the relative abundances of the microbiota species at the genus level by the Bray-Curtis distances was shown in Fig. 2.

Principal component analysis based on the gene level (Fig. 3a) and KEGG profile (Fig. 3b) demonstrated that the gut microbiome of AGM_P and AGM_N can be clearly distinguished from that of CM and RM. And the CM gut microbiome is closer to the RM microbiome than the AGM microbiome (Fig. 3). The distribution of CAZy classes between different groups were shown in Fig. 4a. Compared with CM, the alpha-galactosidase (EC 3.2.1.22), which is involved in lipid metabolism, was significantly downregulated in AGM_N ($P < 0.01$) (Fig.S4&S5). Compared with RM, the beta-glucosylceramidase (EC 3.2.1.45), which is also involved in lipid metabolism, was significantly upregulated in AGM_N ($P < 0.05$) (Fig.S4&S5). The significantly enriched terms by KEGG Orthology between different groups were shown in which the 3-oxoacyl-[acyl-carrier protein] reductase (K00059) and beta-galactosidase (K01190) was related to fatty acid biosynthesis/metabolism and lipid metabolism, respectively (Fig.S6). Differences in the ARO (Antibiotic Resistance Ontology) distribution were shown in Fig. 4b.

Validation of the differential gut microbiota profile of AGM

The most studied microbial metabolites that influence immune system homeostasis are short-chain fatty acids (SCFAs), such as acetate, propionate and butyrate. Among SCFAs, butyrate has multiple regulatory roles at the gut level, exerting an anti-inflammatory effect on both intestinal epithelial cells and immune cells, and influence host gut health [34, 35]. Several bacteria, such as *Coprococcus catus*, *Eubacterium rectale*, *Eubacterium hallii*, *Faecalibacterium prausnitzii*, *Roseburia spp*, produce butyrate [36].

To validate the profiling data, further analysis of feces samples from 20 AGM_N and 20 CM via quantitative RT-PCR demonstrated that AGM_N possessed a lower abundance of *Bifidobacteria* ($P < 0.01$), a higher abundance of *Prevotella* ($P > 0.05$) the butyrate-producing *Faecalibacterium prausnitzii* ($P < 0.01$)

and *Eubacteria* ($P < 0.05$) (Fig. 5). Compared with SIV- AGM, SIV + AGM possessed a higher abundance of *Bifidobacteria* ($P < 0.05$) and *Prevotella* ($P > 0.05$) (Fig. 5).

Comparison of the metabonomic profiles between AGM_N and CM

There were altogether 255 positive and 176 negtive metabolites identified with significantly different levels between AGM_N and CM group (Fig. 6, Table 2).The KEGG pathway annotation of the negtive metabolites and positive metabolites between AGM_N and CM demonstrated that the top 2 annotated KEGG pathways were amino acid metabolism and lipid metabolism (Fig.S7). The lipidmaps annotation of the negtive metabolites and positive metabolites between AGM_N and CM indicated that fatty acids and conjugates, flavonoids, steroids were the top 3 annotated lipids (Fig.S8). The most enriched terms of by KEGG Orthology between AGM_N and CM are biosynthesis of unsaturated fatty acids, carbon metabolism, biosynthesis of amino acids, galactose metabolism for the negtive metabolites as well as metabolic pathways, steroid hormone biosynthesis, vitamin digestion and absorption, glycerophospholipid metabolism for the positive metabolites (Fig. 7).

Table 2
Numbers of the metabolites at significantly different levels, either with positive ions or negative ions, were compared between AGM_P, AGM_N, CM.

Compared samples	Number of total identified metabolites	Number of upregulated metabolites	Number of downregulated metabolites
AGM_N vs CM_pos	255	94	161
AGM_N vs CM_neg	176	76	100
AGM_P vs AGM_N_pos	63	9	54
AGM_P vs AGM_N_neg	22	3	19

Next, correlation between metabolites, as well as correlation between metabolite and microbiota species, was analysed. Among the negtive metabolites, the gentisic acid (Com 1389), which is related to pyruvate metabolism and butanoate metabolism, was found to be at higher levels and positively correlated to LPC 16:0 (Com 1188), LPC 18:2 (Com 2871), LPG 16:0 (Com 349), LPG 15:0 (Com 282), LPG 17:0 (Com 1908), PG (3:0/15:0) (Com 1309) in AGM_N compared to CM (Fig. 8). Among the positive metabolites, LPC 18:3 (Com 3353), PC 14:1e/3:0 (Com 7743), PC 14:1e/4:0 (Com 256), LPC 14:0 (Com 956), PC 14:1e/6:0 (Com 6270) were found to be at higher levels in AGM_N compared to CM (Fig.S9). All the above metabolites were negatively correlated to the abundances of Haloarchaeobius, Methanobrevibacter, and

Methanothermococcus in AGM_N (Fig. 9). These results indicated decreased capacity in lipid metabolism as well as increased capacity in butanoate metabolism in AGM_N compared with CM.

Comparison of the gut microbiota and metabonomic profiles between AGM_P and AGM_N

Clear changes in the gut microbiome composition have been reported between HIV-infected and uninfected individuals both in the early and chronic infection stage [37]. Although the fecal microbiota of healthy humans and macaques shares many similarities, there was not such strong clustering of bacterial communities associated with SIV infection as that in HIV infection [38]. Compared with CM, our data demonstrated an significant enrichment in *Prevotella* and Ruminococcaceae and decreased abundances of Bacteroides, *Alistipes*, *Lactobacillus* and *Streptococcus* in the gut microbiome composition of AGM_N, resembling a trend as found in early SIV infection [39] as well as in chronic HIV infection [41–43]. Compared with AGM_N, a trend in the increased abundances of *Streptococcus* and *Roseburia* were shown in AGM_P (Fig.S3). Compared with AGM_N, most of the lipid metabolites were found to be at lower levels in AGM_P and positively correlated to each other (Fig.S11, S12, S13, S14), indicating an increased capacity in lipid metabolism in AGM during chronic SIV infection. LPE 20:1 (Com 6182) and PE 16:2e/16:1 (Com 15213) were positively correlate to the microbiota species ,such as Methanoregula, in AGM_P (Fig.S15).

Discussion

NHPs share similar characteristics in many aspects to humans when they are used in models of neuroscience, infectious diseases and drug safety testing. Differences also exist between NHP species such as CM and AGM. AGM are resistant to AIDS progression caused by simian immunodeficiency virus and can be used as a model of spontaneous hypertension. Besides, genetic differences between CM and AGM influence the diet responsiveness. However, the mechanisms in shaping their specific biological features remain not clearly understood.

Natural hosts have co-evolved with SIV and are capable of avoiding disease progression. The mechanisms of this phenotype may diverge. Unlike AGM, sooty mangabey (SM) maintains healthy frequencied of CD4 + T cells and genome sequencing has identified two gene products (ICAM-2 and TLR-4), which show structural differences that may influence cell-surface expression (ICAM-2) and downstream signalling (TLR-4) [44]. In AGM, the co-evolution with SIVagm may be accounted for partially by the development of $CD4^{-}CD8a^{dim}$ T-cells from memory $CD4^{+}$ T-cells. Like other natural hosts of SIV, CD4-like immunological functions can be elicited by $CD4^{-}$ T-cells in AGM [45] and preservation of $CD4^{+}$ T-cell function may contribute to the lack of immune activation in AGM and SM [46, 47]. By assessing gene expression profiles from acutely SIV infected AGM and RM, a recent study found that AGM rapidly activate and maintain evolutionarily conserved regenerative wound healing mechanisms in mucosal tissue, which preserves mucosal integrity and prevents inflammatory insults that underlie immune

exhaustion in RM [24]. The most studied microbial metabolites that influence immune system homeostasis are short-chain fatty acids (SCFAs), such as acetate, propionate and butyrate. Among SCFAs, butyrate has multiple regulatory roles at the gut level, exerting an anti-inflammatory effect on both intestinal epithelial cells and immune cells, and influence host gut health [30, 31]. Several bacteria, such as *Coprococcus catus*, *Eubacterium rectale*, *Eubacterium hallii*, *Faecalibacterium prausnitzii*, *Roseburia spp*, produce butyrate [32]. In this study, profiles and possible roles of the AGM gut microbiome and metabolites in shaping these differences are investigated.

Our data confirmed that AGM possessed a higher abundance of the butyrate-producing Clostridium, *Ruminococcus, Eubacterium, Roseburia*, and *Faecalibacterium*, indicating an enhanced ability in facilitating immune system homeostasis and mucosal integrity. Also, AGM possessed a higher abundance of *Blautia* which belongs to the family of *Lachnospiraceae* and classified as beneficial of which administration can attennuates obesity, inflammation and dysbiosis [48]. Upon SIV infection, AGM exhibited an significant enrichment in *Prevotella* and *Ruminococcaceae* and decreased abundances of *Bacteroides*, *Alistipes*, *Lactobacillus* and *Streptococcus* in the gut microbiome composition, resembling a trend as found in early SIV infection [39] as well as in chronic HIV infection [41–43]. Upregulation of several metabolites, such as the butanoate metabolism-related gentisic acid, the anti-inflammatary FAHFA (fatty acid hydroxy fatty acids), in AGM also correlates with findings in the gut microbiome composition. Differences in metabolites involved in lipid metabolism between AGM and CM suggest their different capacities in lipid metabolism. Intersetingly, AGM with chronic SIV infection demonstrated enhanced activity in lipid metabolism compared with SIV- AGM, suggesting a possible role of lipid metabolism in adaption to SIV infection. All these results reflect a natural selection pressure of SIV infection and evolutionary adaption of the AGM as a natural host of SIV to avoid AIDS progression.

Conclusions

Compared with CM and RM, AGM possesses different capacities of lipid metabolism and butanoate metabolism, which correlates with gut homeostasis and mucosal integrity. These findings may provide insight into AIDS resistance in AGM.

Declarations

Funding

This study was funded by the National Projects of Infectious Disease under Grant No.2017ZX10304402003.

Avaliability of data and materials

Please contact author for data requests.

Authors' contributions

XZ conceived and designed the experiments. XZ, JW, YS, SW performed experiments. XZ, YQ, ZY analyzed the data and wrote the paper. All authors read and approved the final manuscript.

Ethics approval and consent to participate

Not applicable.

Consent for publication

Not applicable.

Competing interests

All authors declare that they have no competing interests.

Author details

Laboratory Animal Center, the Academy of Military Medical Sciences, Beijing 100071, People's Republic of China.

References

1. Savage DC. Microbial ecology of the gastrointestinal tract. AnnuRevMicrobiol. 1977;31:107–33.
2. Sonnenburg JL, Backed F. Diet-microbiota interactions as moderators of human metabolism. Nature. 2016;535:56–64.
3. Kostic AD, Xavier RJ, Gevers D. The microbiome in inflammatory bowel disease: current status and the future ahead. Gastroenterology. 2014;146:1489–99.
4. Mitre E, Susi A, Kropp LE, Schwartz DJ, Gorman GH, et al.Association Between Use of Acid-Suppressive Medications and Antibiotics During Infancy and Allergic Diseases in Early Childhood. JAMA Pediatr.2018;172,e180315.
5. Belkaid Y, Hand TW. Role of the microbiota in immunity and inflammation. Cell. 2014;157:121–41.
6. Carabotti M, Scirocco A, Maselli MA. Severi C.The gut-brain axis:interactions between enteric microbiota, central and enteric nervous systems. AnnGastroenterol. 2015;28:203–9.
7. Foster JA, McVey Neufeld KA. Gut-brain aixs: how the microbiome influences anxiety and depression. Trends Neurosci. 2013;36(5):305–12.
8. Klatt NR, Cheu R, Birse K, Zevin AS, Perner M, et al. Vaginal bacteria modify HIV tenofovir microbicide efficacy in African women. Science. 2017;356:938–45.
9. Gopalakrishman V, Spencer CN, Nezi L, Reuben A, Andrews MC, et al. Gut microbiome modulates response to anti-PD-1 immunotherapy in melanoma patients. Science. 2018;359:97–103.
10. Routy B, Le Chatelier E, Derosa L, Duong CPM, Alou MT, Daillere R, et al. Gut microbiome influences efficacy of PD-1-based immunotherapy against epithelial tumors. Science. 2018;359:91–7.

11. Xiao L, Feng Q, Liang S, Sonne SB, Xia Z, Qiu X, et al. A catalog of the mouse gut metagenome. Nat Biotechnol. 2015;1(10):1103–8.
12. Lagkouvardos I, Pukall R, Abt B, Foesel BU, Meier-Kolthoff, Kumar N, et al. The Mouse Intestinal Bacterial Collection (miBC) provides host-specific insight into cultured diversity and functional potential of the gut microbiota. Nature Microbiology. 2016;1(10):16131.
13. Nguyen TL, Vieira-Silva S, Liston A, Raes J. How informative is the mouse for human gut microbiota research? Dis Model Mech. 2015;8(1):1–16.
14. Carlsson HE, Schapiro SJ, Farah I, Hau J. Use of primates in research: a global overview. Am J Primatol. 2004;63(4):225–37.
15. Osada N, Hirata M, Tanuma R, Suzuki Y, Sugano S, Terao K, et al. Collection of Macaca fascicularis cDNAs derived from bone marrow, kidney, liver, pancreas, spleen, and thymus. BMC Res Notes. 2009;2:199.
16. Ebeling M, Kung E, See A, Broger C, Steiner G, Berrera M, et al. Genome-based analysis of the nonhuman primate Macaca fascicularis as a model for drug safety assessment. Genome Res. 2011;21(10):1746–56.
17. Jones SM, Feldmann H, Stroher U, Geisbert JB, Fernando L, Grolla A, et al. Live attenuated recombinant vaccine protects nonhuman primates against Ebola and Marburg viruses. Nat Med. 2005;11(7):786–90.
18. Geisbert TW, Hensley LE, Larsen T, Young HA, Reed DS, Geisbert JB, et al. Pathogenesis of Ebola Hemorrhagic Fever in Cynomolgus Macaques. Am J Pathol. 2003;163(6):2347–70.
19. Fukasawa M, Miuta T, Hasegawa A, Morikawa S, Tsujimoto H, Miki K, et al. Sequence of simian immunodeficiency virus from African green monkey, a new member of the HIV/SIV group. Nature. 1988;333(6172):457–61.
20. Apetrei C, Robertson DL, Marx PA. The history of SIVS and AIDS:epidemiology, phylogeny and biology of isolates from naturally SIV infected non-human primates (NHP) in Africa. Frontiers in bioscience:a journal virtual library. 2004;9:225–54.
21. Renna NF, de Las Heras N, Miatello RM. Pathophysiology of vascular remodeling in hypertension. Int J Hypertens. 2013;2013:808353.
22. RHoads MK, Goleva SB, Beierwaltes WH, Osborn JL. Renal vascular and glomerular pathologies associated spontaneous hypertension in the nonhuman primate Chlorocebus aethiops sabaeus. Am J Physiol Regul Integr Comp Physiol Sep. 2017;1(3):R211–8. 313(.
23. Rudel LL. Genetic factors influence the atherogenic response of lipoproteins to dietary fat and cholesterol in nonhuman primates. J Am Coll Nutr. 1997;16(4):306–12.
24. Barrenas F, Raehtz K, Xu C, Law L, Green RR, Silvestri G, et al. Macrophage-associated wound healing contributes to African green monkey SIV pathogenesis. Nat commun. 2019;10:5101.
25. Clayton JB, Vangay P, Huang H, Ward T, Hillmann BM, Al-Ghalith GA, et al. Captivity humanizes the primate microbiome. Proc Natl Acad Sci USA. 2016;113(37):10376–81.

26. Angelakis E, Yasir M, Bachar D, Azhar E, Lagier JC, Bibi F, et al. Gut microbiome and dietary patterns in different Saudi populations and monkeys. Sci Rep. 2016;6:32191.
27. He X, Slupsky CM, Dekker JW, Haggarty NW, Lonnerdal B, et al. Intergrated role of Bifidobacterium animalis subsp.lactis supplementation in gut microbiota, immunity, and metabolism of infant rhesus monkeys. mSystems. 2016;1(6):e00128-16.
28. Hale VL, Tan CL, Niu K, Yang Y, Knight R, Zhang Q, et al. Diet versus phylogeny: a comparison of gut microbiota in captive colobine monkey species. Microb Ecol. 2018;75(2):515–27.
29. Li W, Godzik A. Cd-hit: a fast program for clustering and comparing large sets of protein or nucleotide sequences. Bioinformatics. 2006;22(13):1658–9.
30. Buchfink B, Xie C, Huson DH. Fast and sentitive protein alignment using DIAMOND. Nat Methods. 2015;12:59–60.
31. Li X, Liang S, Xia Z, Qu J, Liu H, Liu C, et al. Establishment of a Macaca fascicularis gut microbiome gene catalog and comparison with the human, pig, and mouse gut microbiomes. GigaScience. 2018;7:1–10.
32. Qin N, Zheng B, Yao J, Guo L, Zuo J, Wu L, et al. Influence of H7N9 virus infection and associated treatment on human gut microbiota. Sci Rep. 2015;5:14771.
33. Bray JR, Curtis JT. An ordination of the upland forest communities of southern Wisconsin. Ecol Monogr. 1957;27:325–49.
34. Cavaglieri CR, Nishiyama A, Fernandes LC, Curi R, Miles EA, Calder PC. Differential effects of short-chain fatty acids on proliferation and production of pro- and anti-inflammatory cytokines by cultured lymphocytes. Life Sci. 2003;73(13):1683–90.
35. Segain JP, Raingeard de la Bletiere D, Bourreille A, Leray V, Gervois N, Rosales C, et al. Butyrate inhibits inflammatory responses through NFkappaB inhibition: implications for Crohn's disease. Gut. 2000;47(3):397–403.
36. Duncan SH, Barcenilla A, Stewart CS, Pryde SE, Flint HJ. Acetate utilization and butyryl coenzyme A (CoA) transferase in butyrate-producing bacteria from the human large intestine. Appl Environ Microbiol. 2002;68:5186–90.
37. Crakes KR, Jiang G. Gut Microbiome Alterations During HIV/SIV Infection: Implications fot HIV Cure. Front Microbiol. 2019;10:1104.
38. Klatt NR, Canary LA, Sun X, Vinton CL, Funderburg NT, Morcock DR, et al. Probiotic/prebiotic supplementation of antiretrovirals inproves gastrointestinal immunity in SIV-infected macaques. J Clin Invest. 2013;123:903–7.
39. Vujkovic-Cvijin I, Swainson LA, Chu SN, Ortiz AM, Santee CA, Petriello A, et al. Gut-resident lactobacillus abundance associates with IOD1 inhibition and Th17 dynamics in SIV-infected macaques. Cell Rep. 2015;13:1589–97.
40. Lozupone CA, Li M, Campbell TB, Flores SC, Linderman D, Gebert MJ, et al. Alterations in the gut microbiota associated with HIV-1 infection. Cell Host Microbe. 2013;14:329–39.

41. Dillon SM, Lee EJ, Kotter CV, Austin GL, Dong Z, Hecht DK, et al. An altered intestinal mucosal microbiome in HIV-1 infection is associated with mucosal and systemic immune activation and endotoxemia. Mucosal Immunol. 2014;7:983–94.
42. Ling Z, Jin C, Xie T, Cheng Y, Li L, Wu N, et al. Alterations in the fecal microbiota of patients with HIV-1 infection: an observational study in a chinese population. Sci Rep. 2016;6:30673.
43. McHardy IH, Li X, Tong M, Ruegger P, Jacobs J, Borneman J, et al. HIV Infection is associated with compositional and functional shifts in the rectal mucosal microbiota. Microbiome. 2013;1:26.
44. Palesch D, Bosinger SE, Tharp GK, Vanderford TH, Paiardini M, Chahroudi A, et al. Sooty mangabey genome sequence provides insight into AIDS resistance in a natural SIV host. Nature. 2018;553(7686):77–81.
45. Vinton C, Klatt NR, Harris LD, Briant JA, Sanders-Beer BE, Herbert R, et al. CD4-like immunological function by CD4- T cells in multiple natural hosts of simian immunodeficiency virus. J Virol. 2011;85(17):8702–8.
46. Gordon SN, Klatt NR, Bosinger SE, Brenchley JM, Milush JM, Engram JC, et al. Severe Depletion of Mucosal CD4 + T-cells in AIDS-Free Simian Immunodeficiency Virus-Infected Sooty Mangabeys. J Immunol. 2007;179:3026–34.
47. Brenchley JM, Paiardini M, Knox KS, Asher AI, Cervasi B, Asher TE, et al. Differential Th17 CD4 T-cell depletion in pathogenic and nonpathogenic lentiviral infections. Blood. 2008;112:2826–35.
48. Sartor RB, Montgomery SA, Coleman RA, Ting JP. (2018). The Inhibitory Innate Immune Sensor NLRP12 Maintains a Threshold against Obesity by Regulating Gut Microbiota Homeostasis. Cell Host & Microbe.2018; *12*: 364–378.

Figures

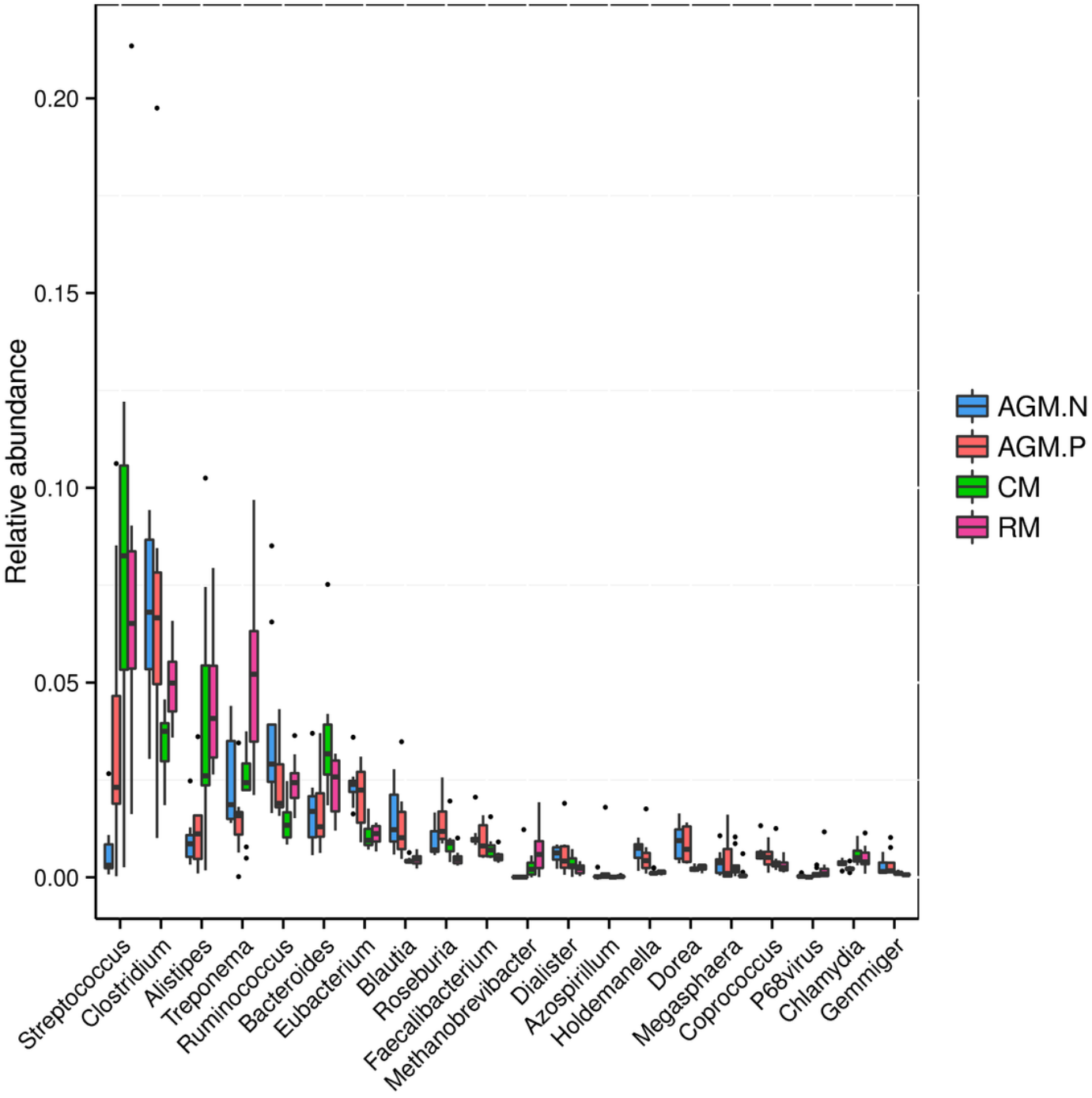

Figure 1

Characteristic of the top 20 genera in the gut microbiota of AGM_P, AGM_N, CM and RM.

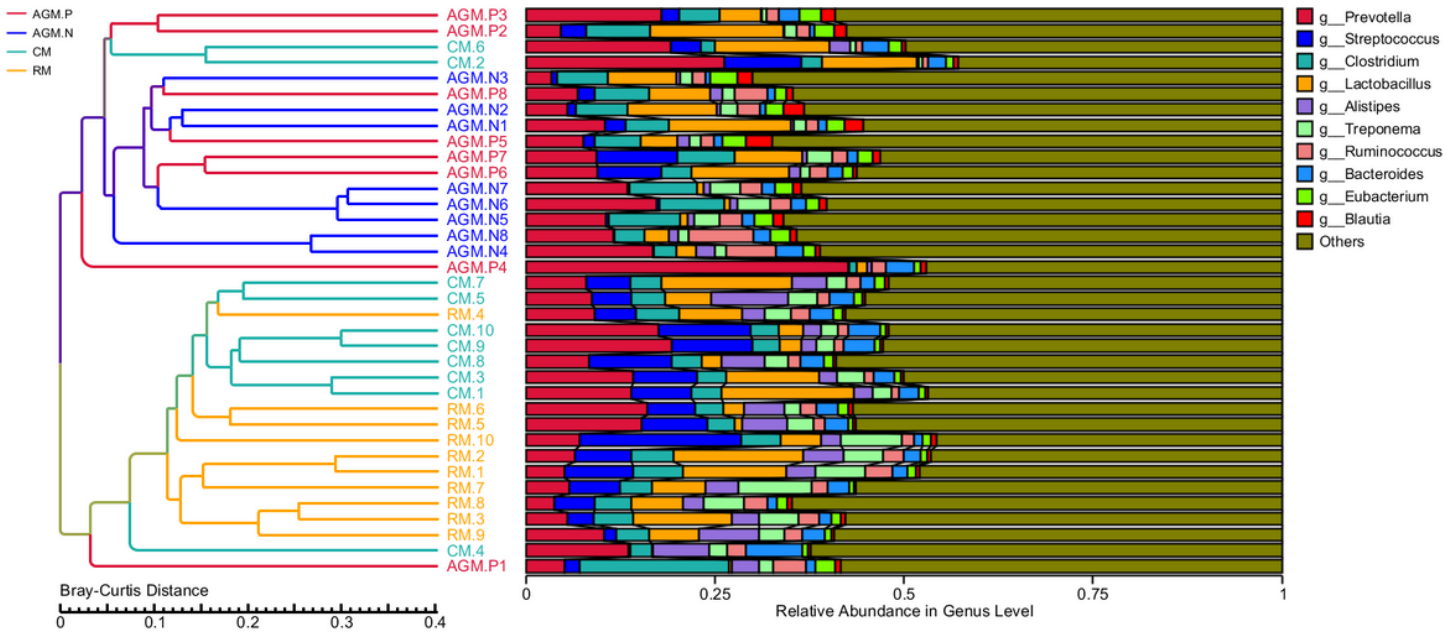

Figure 2

β-diversity display of samples from AGM_P, AGM_N, CM and RM group. Relative abundances in the genus level were compared and distinguished by Bray-Curtis Distance.

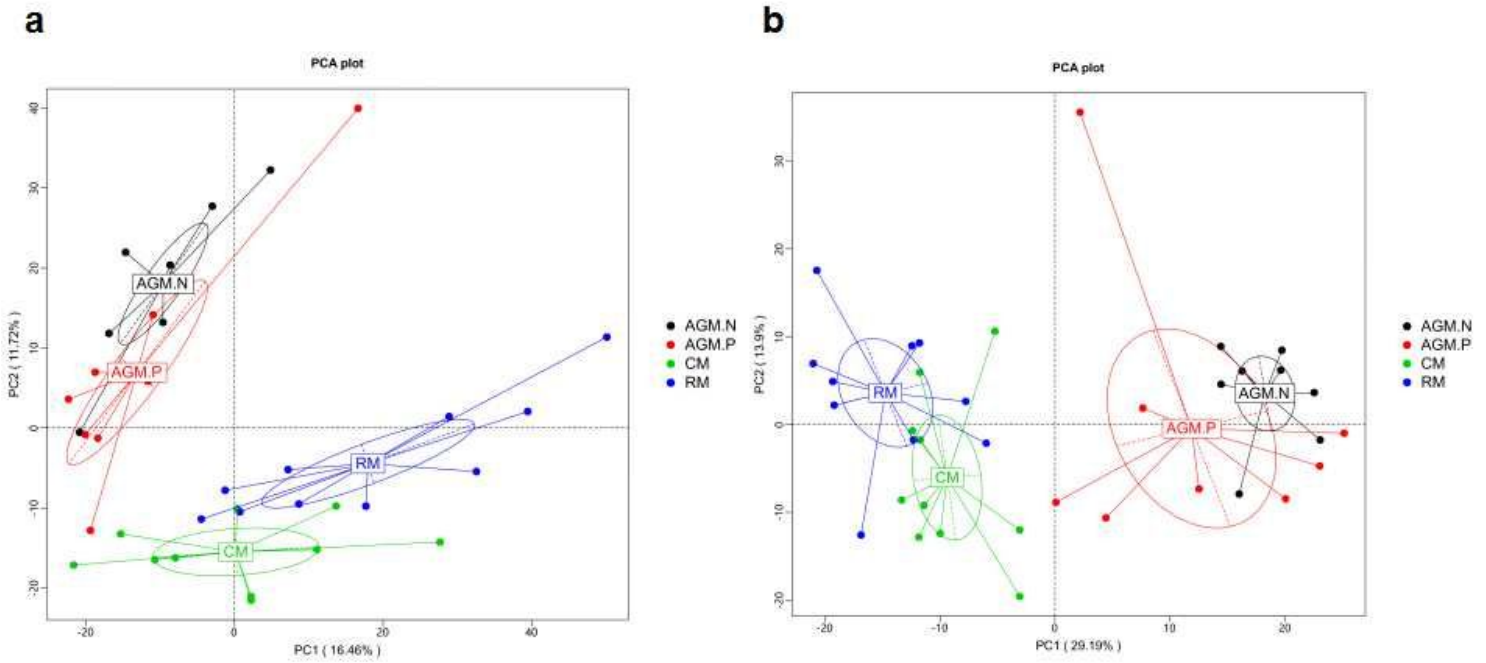

Figure 3

Principal component analysis (PCA) of the gut microbiota of AGM_P, AGM_N, CM and RM. a PCA based on on the gene profiles of the gut microbiota of AGM_P, AGM_N, CM and RM. b PCA based on the KEGG profiles of the gut microbiota of AGM_P, AGM_N, CM and RM.

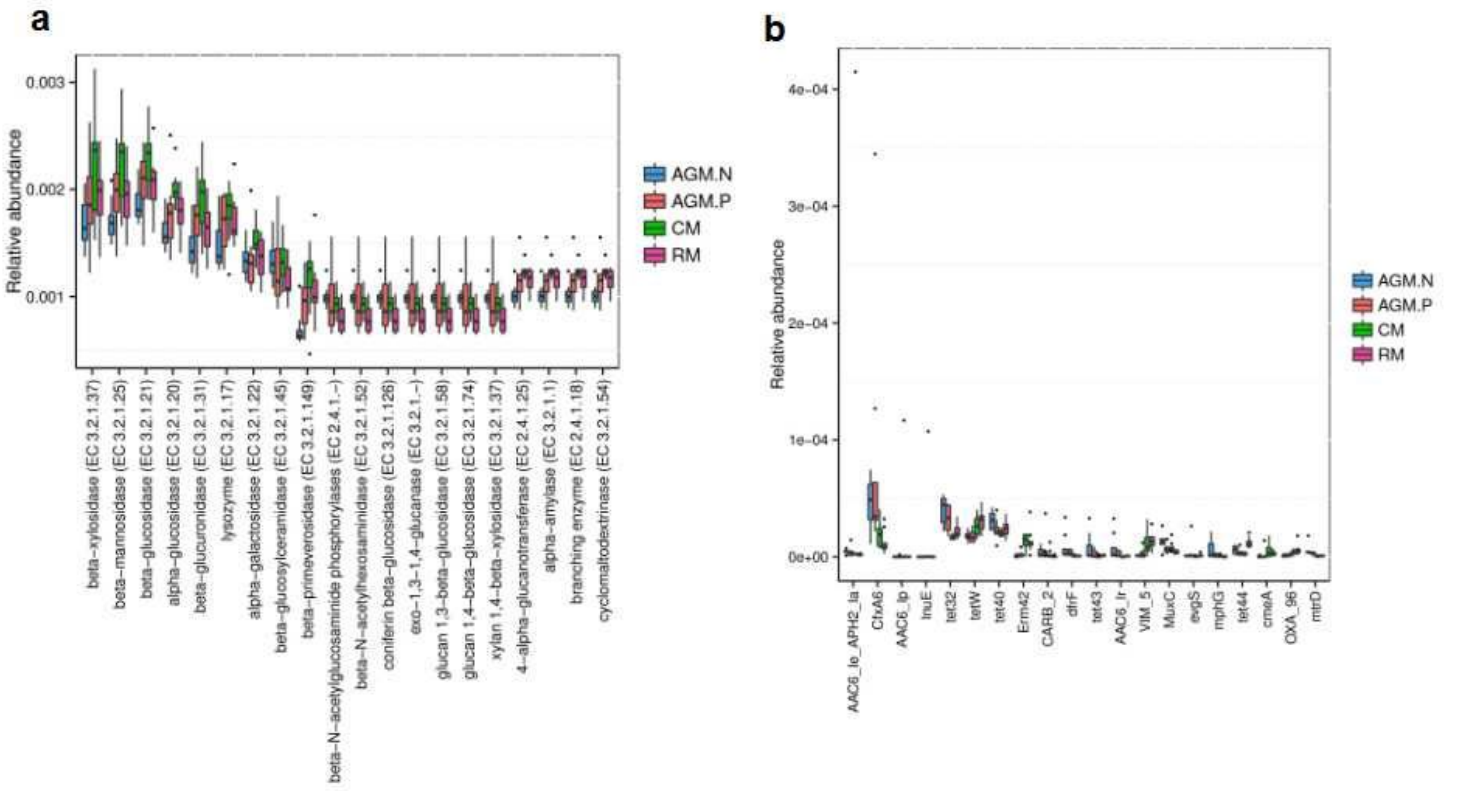

Figure 4

Common functional database annotations based on the amino acid sequences translated from the nucleotide sequences of the gene catalogs of AGM_P, AGM_N, CM and RM. a Functional annotation of the samples by alignment through the CAZy database. b Resistance gene annotation of the samples by alignment through the CARD database.

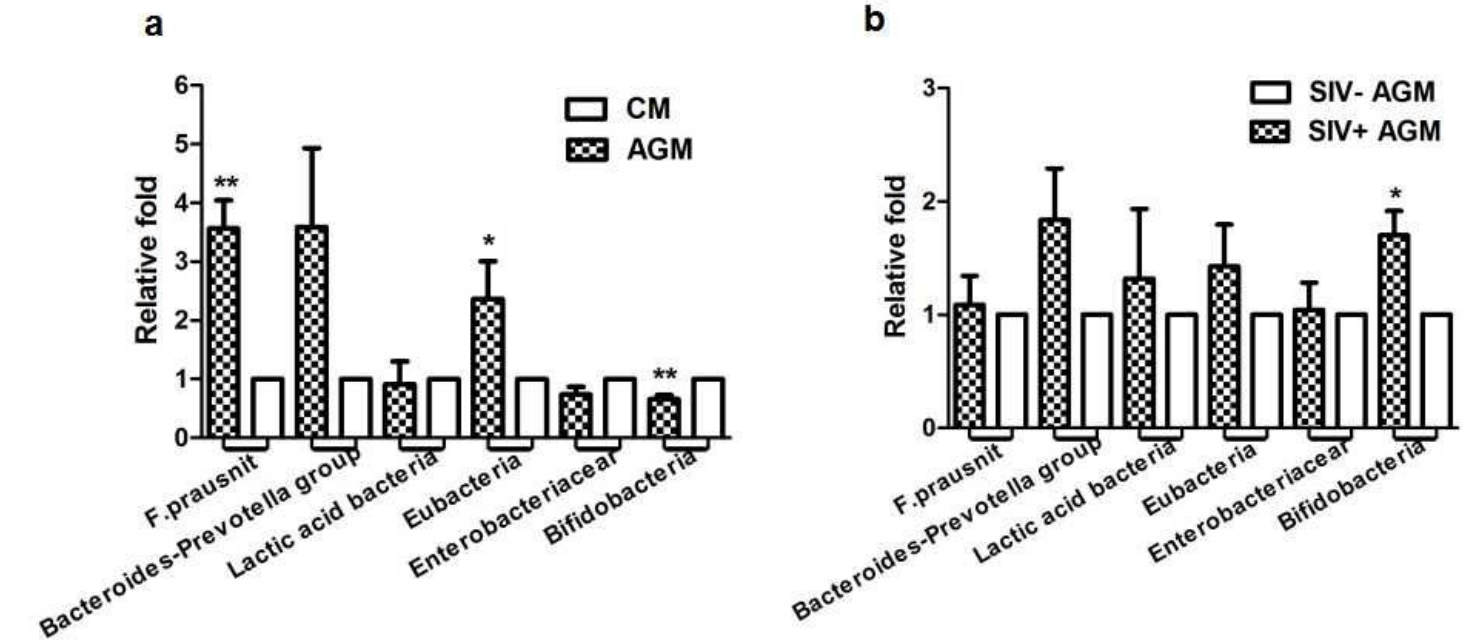

Figure 5

Quantitative RT-PCR analysis of the relative bacterial abundance of feces samples =20from AGM and nCM. a Validation analysis of the relative bacterial abundance of feces samples from SIV- AGM (n=20) and nCM (n=20) via quantitative RT-PCR. b Comparison analysis of the relative bacterial abundance of feces samples from SIV- AGM (n=8) and SIV+ AGM (n=8) via quantitative RT-PCR.

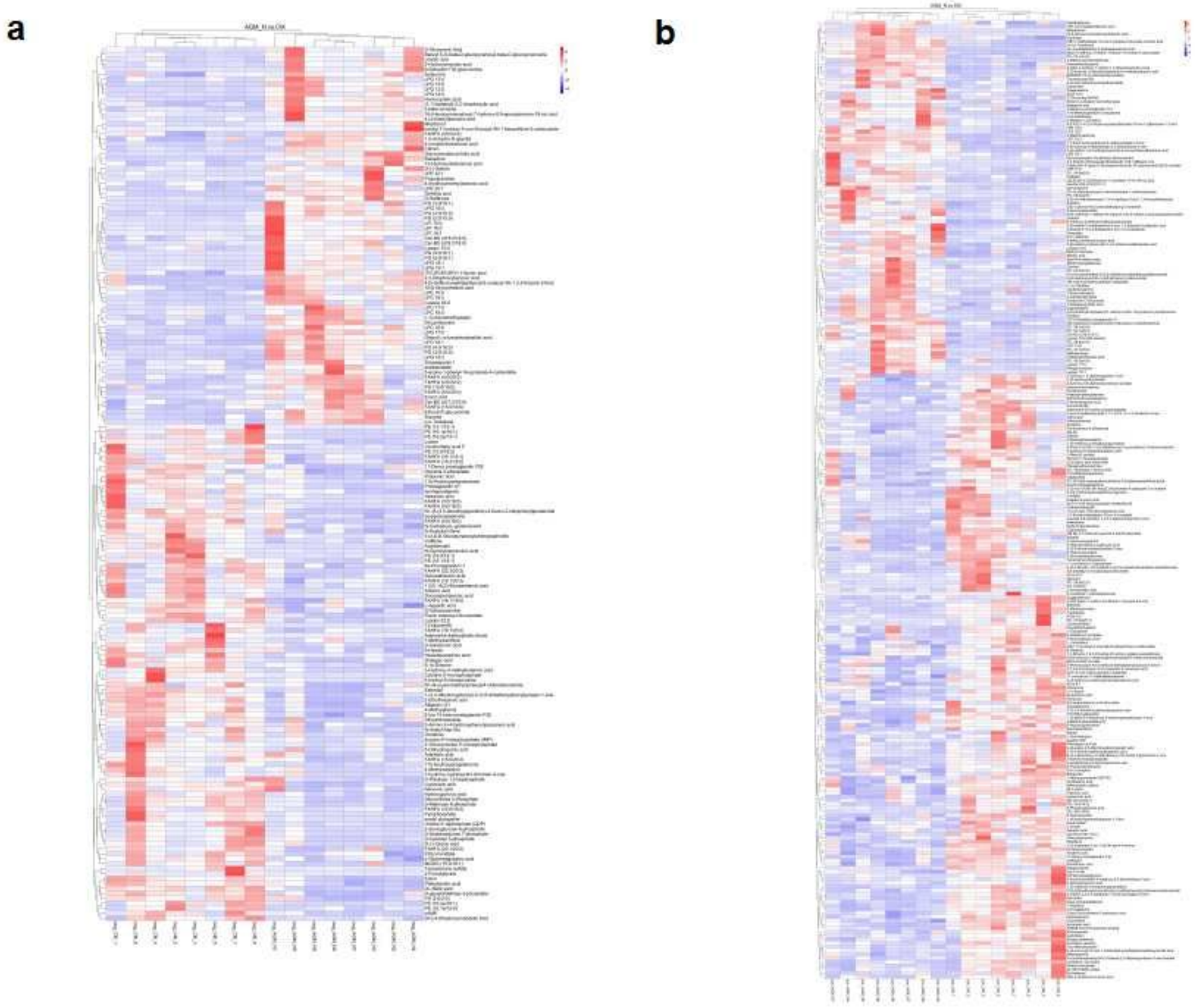

Figure 6

Heatmap comparison of the metabolites identified with significantly different levels between AGM_N and CM group. a Negative metabolites with significantly different levels between AGM_N and CM. b Positive metabolites with significantly different levels between AGM_N and CM. P<0.05 was considered statistically significant.

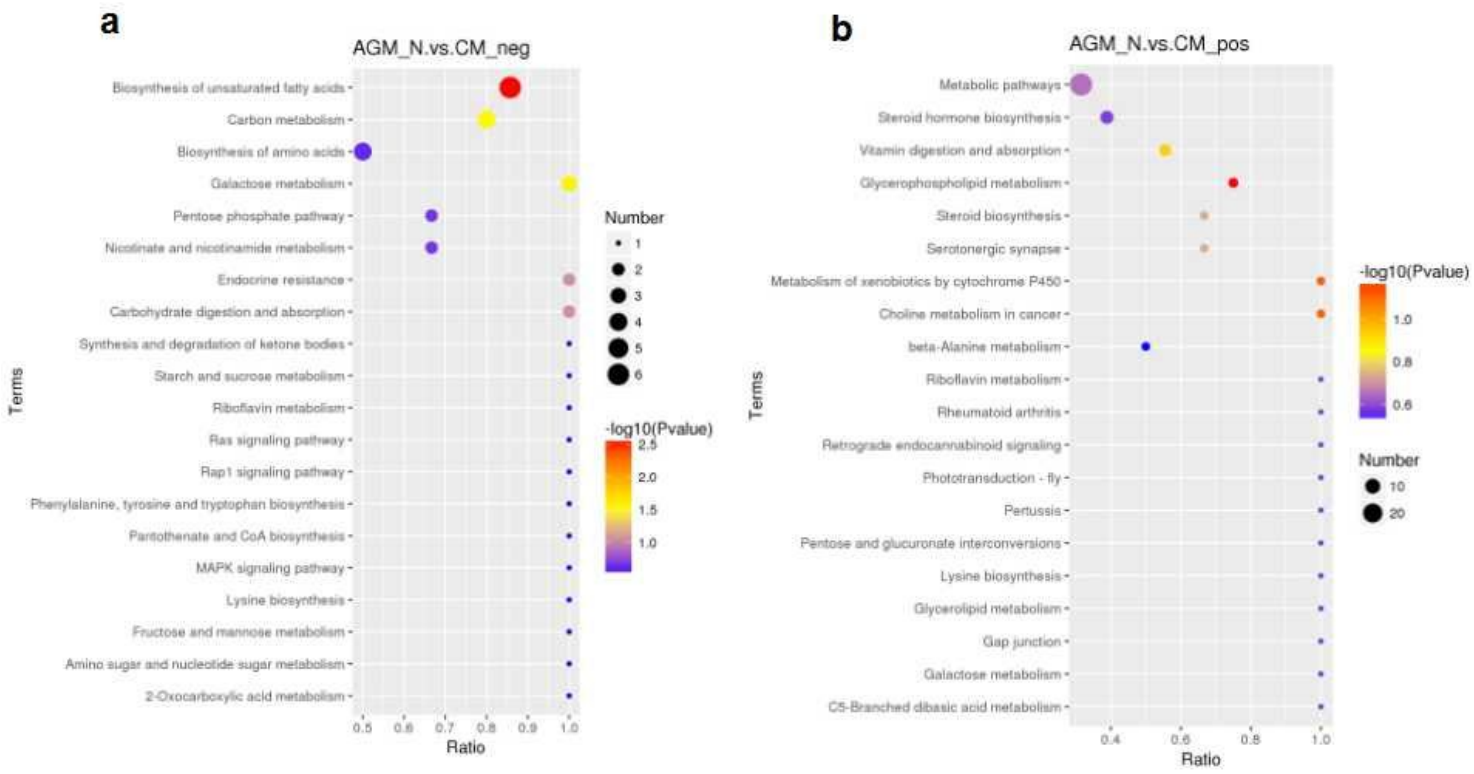

Figure 7

The KEGG enrichment bubble map based on the relative levels of the differential metabolites between AGM_N and CM group. a KEGG map based on the negative metabolites with significantly different levels between AGM_N and CM. b KEGG map based on the positive metabolites with significantly different levels between AGM_N and CM. P<0.05 was considered statistically significant.

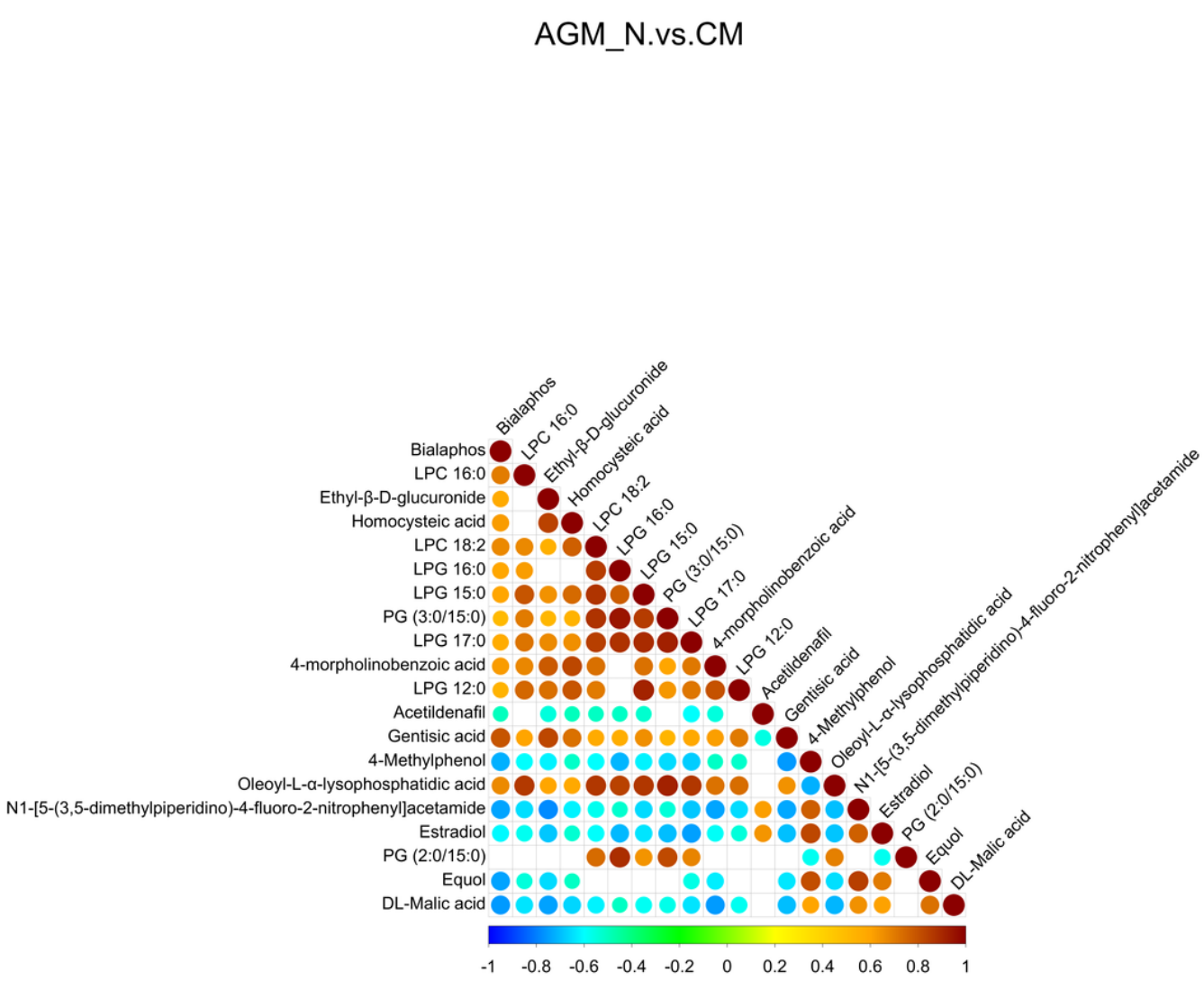

Figure 8

Correlation analysis of the differential levels between the negative metabolites from AGM_N and CM group. P<0.05 was considered statistically significant.

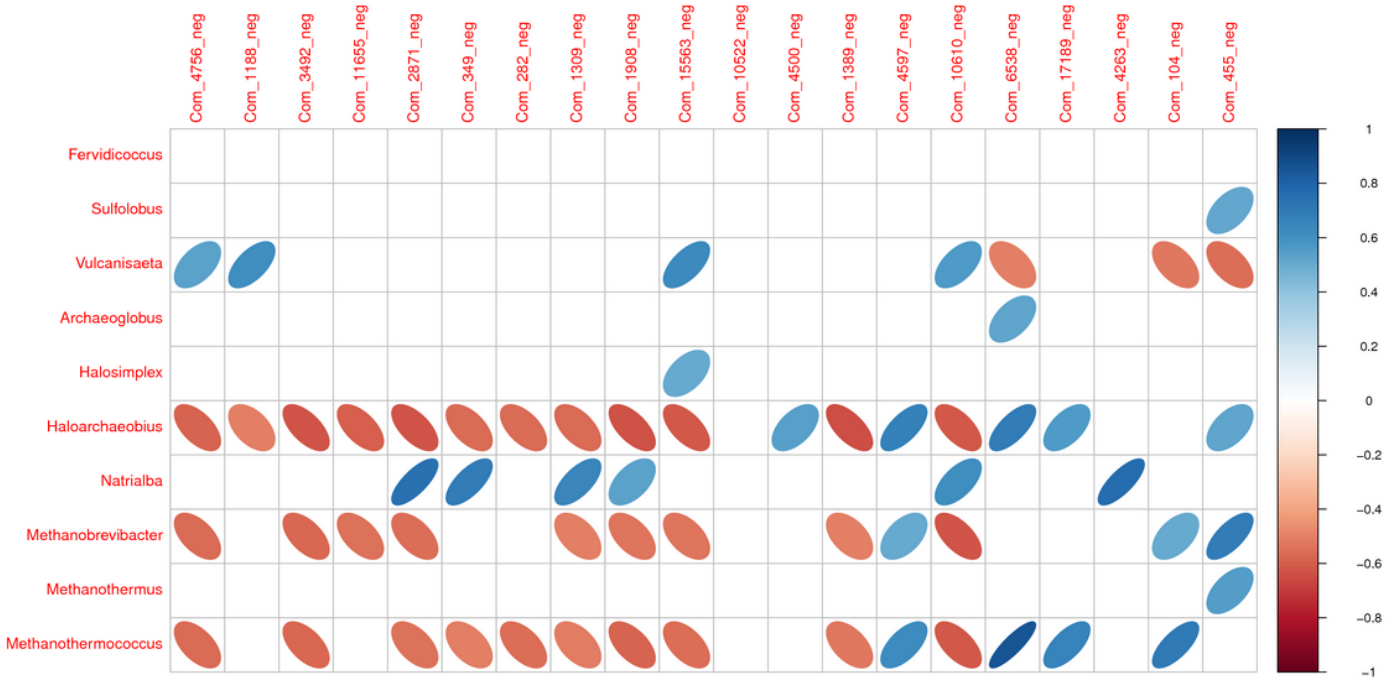

Figure 9

Correlation analysis of negative metabolites with differential levels and the microbiota at genus level between AGM_N and CM group. P<0.05 was considered statistically significant.

Supplementary Files

This is a list of supplementary files associated with this preprint. Click to download.

- SupplementaryFigure15.png
- SupplementaryFigure14.png
- SupplementaryFigure13.png
- SupplementaryFigure12.png
- SupplementaryFigure11.png
- SupplementaryFigure10.png
- SupplementaryFigure9.png
- SupplementaryFigure8.jpg
- SupplementaryFigure7.jpg
- SupplementaryFigure6.png
- SupplementaryFigure5.png
- SupplementaryFigure4.png

- SupplementaryFigure3.png
- SupplementaryFigure2.png
- SupplementaryFigure1.png